J. Membrane Biol. 38, 209–232 (1978)

Passive Electrical Properties of Cultured Murine Lymphoblast (L5178Y) with Reference to its Cytoplasmic Membrane, Nuclear Envelope, and Intracellular Phases

Akihiko Irimajiri, Yukio Doida*, Tetsuya Hanai**, and Akira Inouye

Department of Physiology, Kyoto University School of Medicine, Sakyo, Kyoto 606, Japan

Received 16 November 1976; revised 2 June 1977

Summary. Dielectric dispersion measurements over a frequency range 0.01–100 MHz were made with the suspensions of a cultured cell line, mouse lymphoma L5178Y, and an attempt to explain the observed dielectric behavior by taking explicitly into consideration the possible involvement of cell nucleus has been presented.

The use of a conventional "single-shell" model in which the cell is represented by a homogeneous sphere coated with a thin limiting shell phase did not duplicate the observed dispersion curves, whereas a "double-shell" model in which one additional concentric shell is incorporated into the "single-shell" model gave a much better fit between the observed and the predicted dispersion curves. Based on the latter model, we analyzed the raw data of dielectric measurements to yield a set of plausible electrical parameters for the lymphoma cell: $C_M \simeq 1.0\,\mu F/cm^2$, $C_N \simeq 0.4\,\mu F/cm^2$, $\varepsilon_k \simeq 300$, $\kappa_c/\kappa_a \simeq 0.9$, and $\kappa_k/\kappa_c \simeq 0.7$. Here, C_M and C_N are the specific capacities of plasma and nuclear membranes; ε and κ are the dielectric constant and conductivity with subscript a, c and k referring respectively to the extracellular, the cytoplasmic and the karyoplasmic phases.

Although the knowledge of passive electrical properties such as dielectric constant and conductivity of various cellular components (*e.g.*, cell membrane, cytoplasm and nucleus) is claimed to add much to a better understanding of cell functions [24], there have been so far very few studies dealing with nonexcitable cells of animal origin except for erythrocytes, oocytes and Ehrlich ascites cells [17, 19] (for review, *see* Refs. 3, 24, 26). This is due partly to some technical difficulties involved and partly to the sophisticated procedures needed for interpreting the experimental data.

* Department of Biology, Shiga Medical University, Kusatsu, Shiga, Japan.
** Institute for Chemical Research, Kyoto University, Uji, Kyoto-fu 611, Japan.

022-2631/78/0038-0209 $4.80

However, the advent of Pauly-Schwan's theory [21] concerning the dielectric behavior of dispersed "spherical shells" as a model of biological cell suspensions has provided a basis for the analysis of dielectric measurements and has enabled us to estimate the cellular electrical parameters in greater detail. Along this line of approach, we have also reported a practical method of estimation [8], together with its application to synaptosomes [11] and yeast cells [1].

On the other hand, when we deal specifically with an eukaryotic cell which has a sizeable nucleus inside the cell, an *a priori* application thereto of the Pauly-Schwan theory could not be justified any more. In order to overcome this difficulty by any means, the "single-shell" model (Fig. 1*a*) should be modified so as to effectively accommodate the actual cell's morphology, i.e., the presence of a round, large nucleus within the intracellular space. Next to the simplistic model would then be a "double-shell" model such as depicted in Fig. 1*b*. A detailed description of the theory for the latter model will be given in a separate paper[1] (hereafter referred to as Paper *II*).

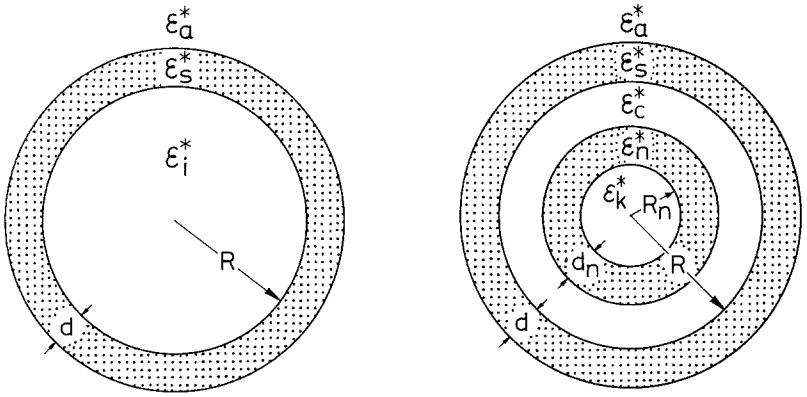

Fig. 1. Two models for a lymphoid cell. The "single-shell" model assumes only one spherical shell (ε_s^*) of thickness d separating the internal phase (ε_i^*) from the ambient (ε_a^*). In the "double-shell" model, the internal phase of the "single-shell" model is subdivided, in a concentric fashion, into the cytoplasmic (subscript c), nuclear envelope (subscript n), and karyoplasmic (subscript k) phases. Asterisk (*) denotes complex dielectric constant, defined as $\varepsilon^* = \varepsilon + \kappa/j\omega\varepsilon_0$, where ε = dielectric constant, κ = conductivity, $j = \sqrt{-1}$, ω = angular frequency and ε_0 = dielectric constant of free space

1 A. Irimajiri, T. Hanai, V. Koizumi, A. Inouye. A dielectric theory of multi-stratified spherical shell model with its application to lymphoma cells *(in preparation)*. A brief account of this work was presented at the 14th Annual Meeting of the Japan Biophysical Society, Osaka, October, 1975 (*Abstr.* p. 340).

In the present paper, we describe first the dielectric dispersions observed with the cultured lymphoma cells (L5178Y) in suspension, and second we shall demonstrate the effectiveness of this new model in analyzing the raw data to obtain the electrical parameters such as dielectric constants and conductivities of cell membrane, cytoplasm, nuclear membrane and karyoplasm. The meaning of the parameter values thus derived is discussed in light of their cell physiological relevance.

Materials and Methods

Cell Culture and Suspending Media

L5178Y cells were grown in Fischer's medium (Nissui Seiyaku Co., Tokyo, Japan) supplemented with 10% bovine serum. The doubling time of the mixed population was 10.5 hr at 37 °C. Cell viability was monitored occasionally by a dye-exclusion test using eosin Y [6] and found to be better than 95%. When the cell count reached around 3×10^5 cells/ml, the cells were collected by low speed centrifugation ($800 \times g$, 3 min), washed once with a serum-free Fischer's, and then resuspended in more than 100 vol of the media of the desired composition. After standing for 10 min in the test medium at 25 °C, the suspension was centrifuged to separate it into cell pellet and supernatant; both the supernatant recovered and the pellet appropriately diluted with the same supernatant were immediately subjected to dielectric measurements.

Three suspending media were used: 1×, 1/2×, and 1/3× Fischer's, designated according to dilution with respect to the original Fischer's medium. The standard medium was an undiluted Fischer's containing 10% (w/v) Ficoll (Pharmacia Fine Chemicals, Uppsala, Sweden; mol wt, 4×10^5); the modified ones were prepared by diluting the standard medium two- or threefold with a buffered Ficoll-sucrose solution (pH 7.3) while maintaining both the final osmolarity and the Ficoll concentration the same as those of the standard medium, i.e., 310 ± 10 mosM and 10%, respectively. The purpose of adding a polysucrose, Ficoll, was to retard cell sedimentation during dielectric measurements by raising the viscosity as well as the density of suspensions. The use of Ficoll in such a concentration proved fairly effective for this purpose, and it hardly ever affected the morphology of cells for at least 30 min within which a single experiment was completed.

The final volume concentration of cell suspensions, estimated conductometrically [10], was adjusted usually to a value between 10 and 20%.

Dielectric Measurements and Corrections

Dielectric constants and conductivities were measured by an Ando Transformer Ratio-Arm Bridge type TR-1BK covering a frequency range 0.01 to 2 MHz, and by a Boonton RX-Meter type 250 A for a range 0.5 to 100 MHz. The Ando bridge was calibrated against a General Radio Precision Capacitor type 1422-CB and a General Radio Decade Resistor type 1433-X. Accuracy of the Boonton instrument was accepted as specified by the manufacturer. Consistency between both bridges was carefully checked and confirmed by using small polystyrene capacitors (5 and 10 pF) as working standards. The dielectric cell used was a type of parallel-plate condenser having a sample cavity of

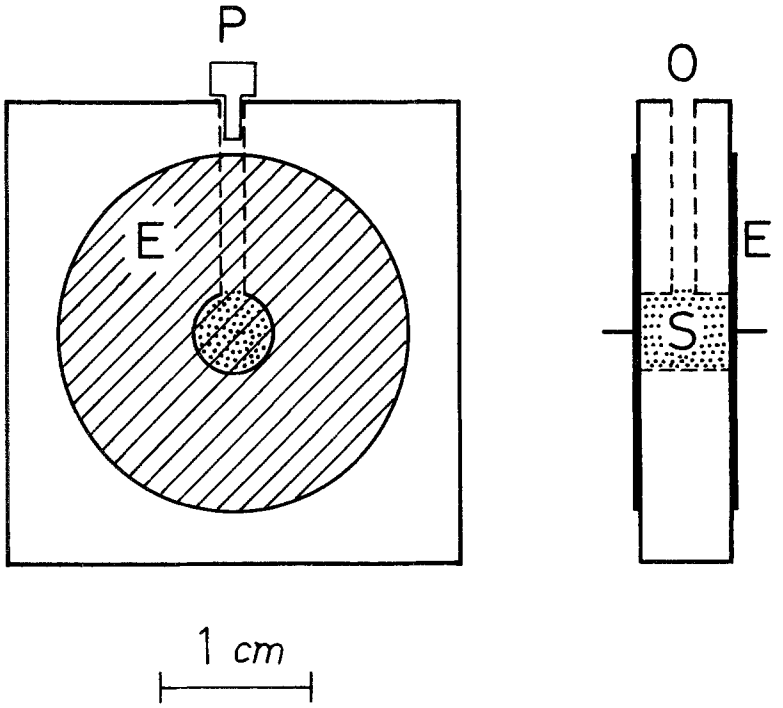

Fig. 2. The dielectric cell used. Pt-coated Pt-disc electrodes (24 mm diameter) were fixed on both sides of a lucite spacer having a cylindrical hole (5 mm bore, 6 mm long) machined at the center. *E*, electrodes; *O*, orifice; *P*, plug; and *S*, sample cavity

0.12 ml; its schematic diagram is shown in Fig. 2. All the measurements were performed at room temperature regulated at 24–26 °C.

Correction was made for the electrode polarization effect which dominated below about 0.1 MHz by means of a frequency variation technique [25]. The series inductance effect was also corrected, according to Schwan's method [25], by applying an inductance value of 2.82×10^{-8} H which was determined with various concentrations of aqueous KCl.

Analysis of Data

Two models for the lymphoid cell as depicted in Fig. 1 were employed in order to explain the observed dielectric behavior of cell suspensions and, in so doing, to determine the component phase parameters. A detailed description of the "single-shell" approach has been reported elsewhere [8]. Briefly, this approach assumes, as the basis of numerical analysis, the following general equation of Pauly and Schwan [21]:

$$\frac{\varepsilon_a^* - \varepsilon^*}{2\varepsilon_a^* + \varepsilon^*} = \frac{(\varepsilon_a^* - \varepsilon_s^*)(2\varepsilon_s^* + \varepsilon_i^*) + (\varepsilon_a^* + 2\varepsilon_s^*)(\varepsilon_s^* - \varepsilon_i^*)(1 + d/R)^{-3}}{(2\varepsilon_a^* + \varepsilon_s^*)(2\varepsilon_s^* + \varepsilon_i^*) + 2(\varepsilon_a^* - \varepsilon_s^*)(\varepsilon_s^* - \varepsilon_i^*)(1 + d/R)^{-3}} \Phi \tag{1}$$

where ε^* is the complex dielectric constant of a cell suspension in which the cells as represented by Fig. 1*a* are dispersed uniformly in a medium of ε_a^* to a volume concentration Φ.

A full explanation of the method based on the "double-shell" model with its theoretical foundation will be given in Paper *II*. In essence, the internal phase of Fig. 1*a* should be electrically equivalent to the spherical domain of radius R in Fig. 1*b*, so that

$$\frac{\varepsilon_c^*-\varepsilon_i^*}{2\varepsilon_c^*+\varepsilon_i^*}=\frac{(\varepsilon_c^*-\varepsilon_n^*)(2\varepsilon_n^*+\varepsilon_k^*)+(\varepsilon_c^*+2\varepsilon_n^*)(\varepsilon_n^*-\varepsilon_k^*)(1+d_n/R_n)^{-3}}{(2\varepsilon_c^*+\varepsilon_n^*)(2\varepsilon_n^*+\varepsilon_k^*)+2(\varepsilon_c^*-\varepsilon_n^*)(\varepsilon_n^*-\varepsilon_k^*)(1+d_n/R_n)^{-3}}\cdot\frac{(R_n+d_n)^3}{R^3}. \quad (2)$$

Thus the dielectric behavior of the "double-shell" model can be expressed by the combination of Eqs. (1) and (2), and these equations were used in the numerical calculations presented below.

In both cases, the most plausible sets of parameters were obtained through a curve-fitting method, in which an overall difference between the observation and the calculated dispersion curves was minimized by changing the cellular phase parameters. Numerical calculations were carried out by a programmable calculator, Yokogawa-Hewlett-Packard Computer Model 10.

Estimation of Morphological Parameters

The mean cellular and nuclear diameters, D $(=2R+2d)$ and D_n $(=2R_n+2d_n)$, were measured on living, unfixed cells fresh from culture by means of a phase contrast microscope. Both values were assessed, on a volume basis, according to the relations:

$$D^3 = \text{arithmetic mean of (cell diameter readings)}^3 \quad (3)$$

$$D_n^3 = D^3 \text{ multiplied by a mean of (nucleus/cell diameter ratios)}^3, \quad (4)$$

because the size parameters are related to the dielectric properties through the "volume" fraction terms as seen from Eqs. (1) and (2).

Determinations of membrane thickness were performed electron microscopically with thin sections prepared by a slight modification of the conventional Luft procedure [16].

Experimental Results

Morphological Parameters

We begin by describing the morphological characteristics of L5178Y cells, since the morphological parameters such as D, D_n, d and d_n have to be known before making analysis for the electrical parameters of the cell.

Phase contrast microscopy (Fig. 3*a*) revealed that the cells were almost ideally spherical with a mean diameter of 13.0 μm. The size distribution was relatively narrow as seen in Fig. 3*b*. These two facts are quite helpful in precluding the possible ambiguity of analysis due to heterogeneity in cell morphology.

The nuclei, also having round contour, occupied 37 % (on an average) in the cell volume as determined by light or electron microscopy, with the exception of the cells in mitotic stage, whose occurrence was usually less than 4 %.

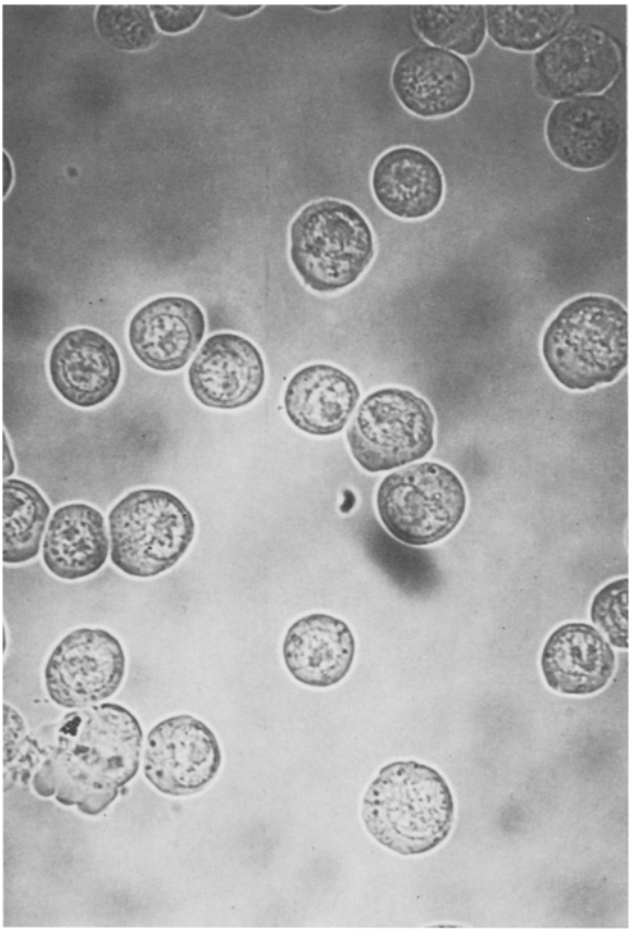

a

Fig. 3. (*a*): Phase contrast micrograph of L 5178 Y cells in Fischer's medium. Magnification, 810×. (*b*): Size distribution obtained with 400 cells

With the aid of electron microscopy (Fig. 4), the values of cellular and nuclear membrane thickness, d and d_n, were estimated. It was also noticed that the fine structure of the nuclear envolope of L5187 Y cells conformed, in all respects, to the ordinary one [7]: (i) the whole envelope consisting of dual layers of unit membrane with an amorphous gap ("cisterna") sandwiched by them, and (ii) frequent occurrence of nuclear "pores" which perforate the full thickness of the envelope. The latter fact makes a cogent support for our finding that the nuclear membrane conductivity κ_n was several orders of magnitude greater than the cytoplasmic membrane conductivity κ_s (*see* Table 2).

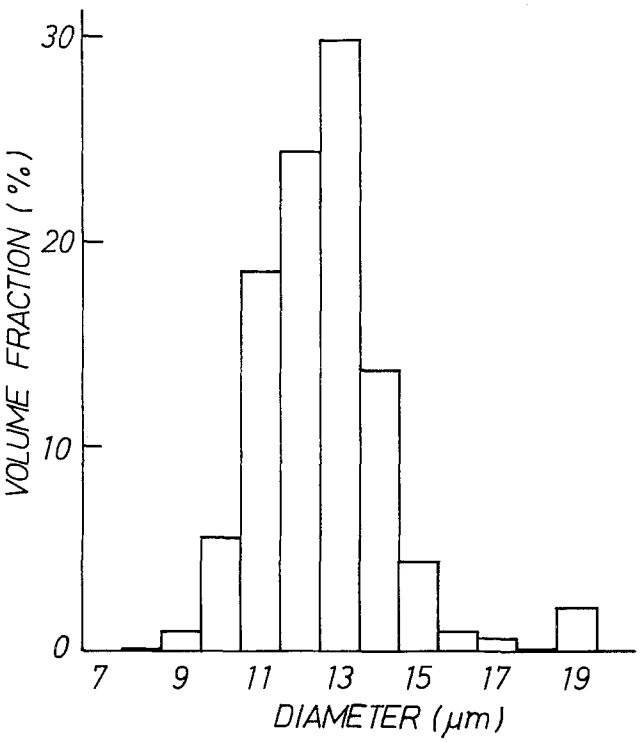

Fig. 3b

The numerical values of the four morphological parameters[2] thus estimated are listed in Table 1, in which are also included some assumed electric parameters necessary for the analysis presented below.

Owing to the manipulated constancy of medium osmolarity around the isotonic one (310 mosM), the cells did not change their gross morphology significantly with changes in the salt concentration tested. To a first approximation, therefore, the same values of the four morphological parameters were used throughout the analyses regardless of varying medium conditions.

Dielectric Behavior

In Fig. 5 are plotted the observed dielectric constants and conductivities, as functions of applied frequency, for a suspension of cells in the standard (1× Fischer's) medium. This figure shows an apparently

2 Of these, the cell membrane thickness d was the most difficult to measure, so that the d-value of 80 Å listed here has been chosen following a convention widely accepted by membrane biologists.

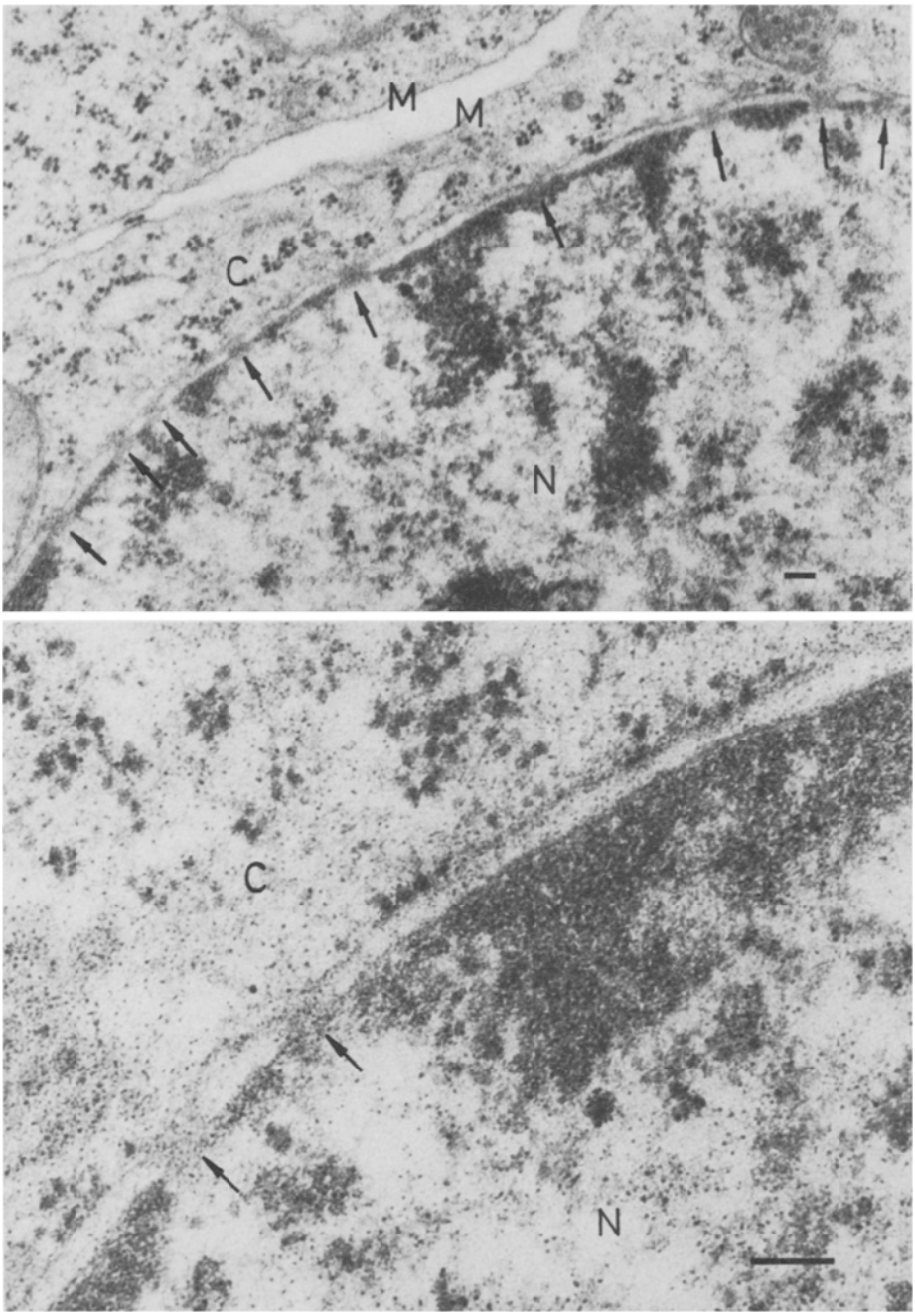

Fig. 4. Electron micrographs of the nuclear envelope of L 5178 Y cells. *Arrow* indicates the nuclear "pore". *M*, cell membrane; *C*, cytoplasm; and *N*, nucleus. Calibration, 1000 Å

Table 1. Parameters employed in the numerical analysis of the observed dispersion curves

Morphological				Electrical[a]	
Diameter		Membrane thickness		Cell membrane conductivity, κ_s (mS/cm)	Cytoplasmic dielectric constant, ε_c
Cellular, D (μm)	Nuclear, D_n (μm)	Cellular, d (Å)	Nuclear, d_n (Å)		
13.0	9.33	80[a]	400	8×10^{-7}[b]	77

[a] Assumed values.
[b] This value corresponds to a specific resistance (with respect to area) of $1\,k\Omega\,cm^2$ for a membrane of 80 Å in thickness.

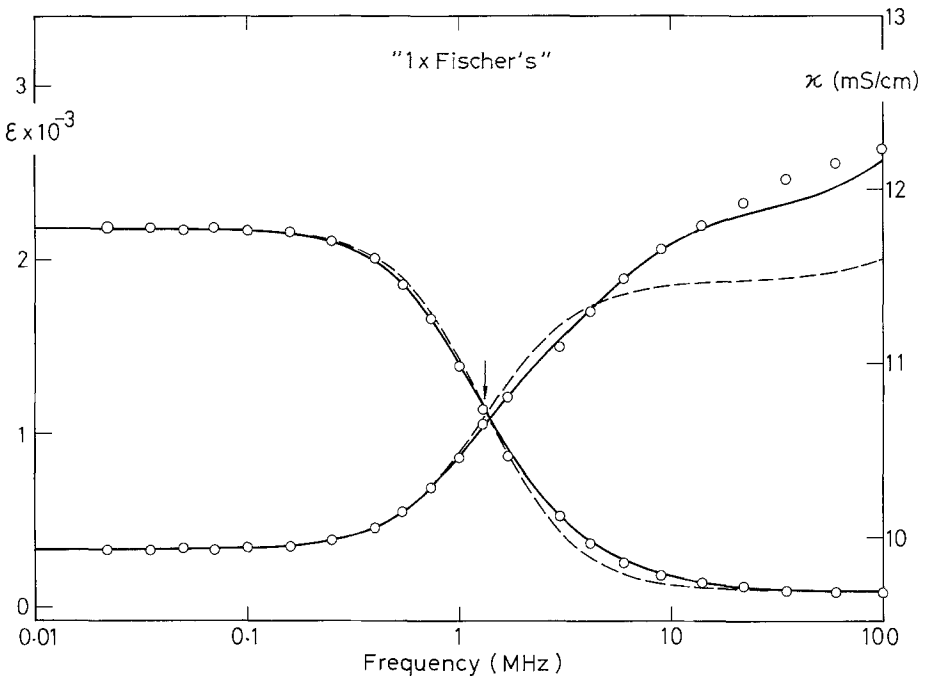

Fig. 5. Plots of dielectric constant (ε) and conductivity (κ), as functions of frequency, for a suspension of L 5178 Y cells in 1 × Fischer's medium. *Solid lines:* the best-fit calculation based on the "double-shell" model for the case of "$\kappa_a = 12.67$ mS/cm" in Table 2. *Dashed lines:* based on the "single-shell" model

typical dielectric dispersion having a characteristic frequency (indicated by *arrow*) of about 1.3 MHz. Fig. 6 shows the complex plane plots of the data presented in Fig. 5. The experimental points trace a circular arc, and its depressed center indicates that the underlying mechanism(s) is not so simple as can be represented by a single relaxation time.

Fig. 7 illustrates a measurement with 1/2 × Fischer's medium, the experimental condition being otherwise similar to that of Fig. 5. The

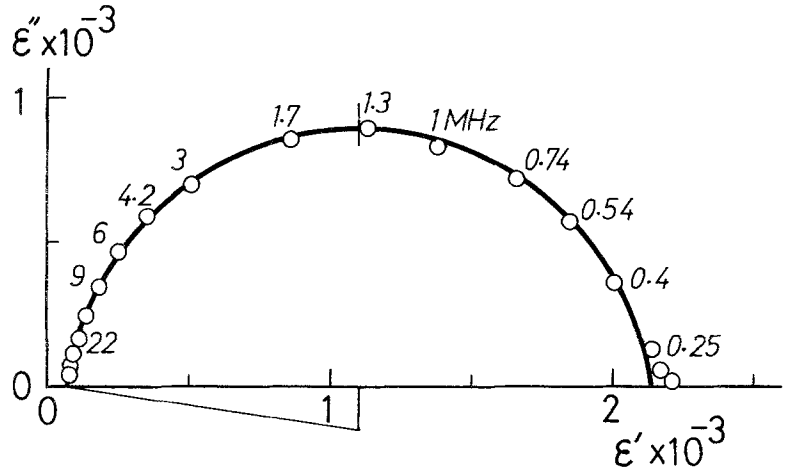

Fig. 6. Complex-plane plot for the data of Fig. 5. The measuring frequency is indicated on each point. *Abscissae:* the real part of complex dielectric constant $\varepsilon^*(=\varepsilon'-j\varepsilon'')$; *Ordinates:* the imaginary part of complex dielectric constant, defined by $\varepsilon''=(\kappa-\kappa_l)\varepsilon_0/\omega$ where κ_l is the limiting conductivity at low frequencies, ε_0 is dielectric constant of free space and ω is angular frequency

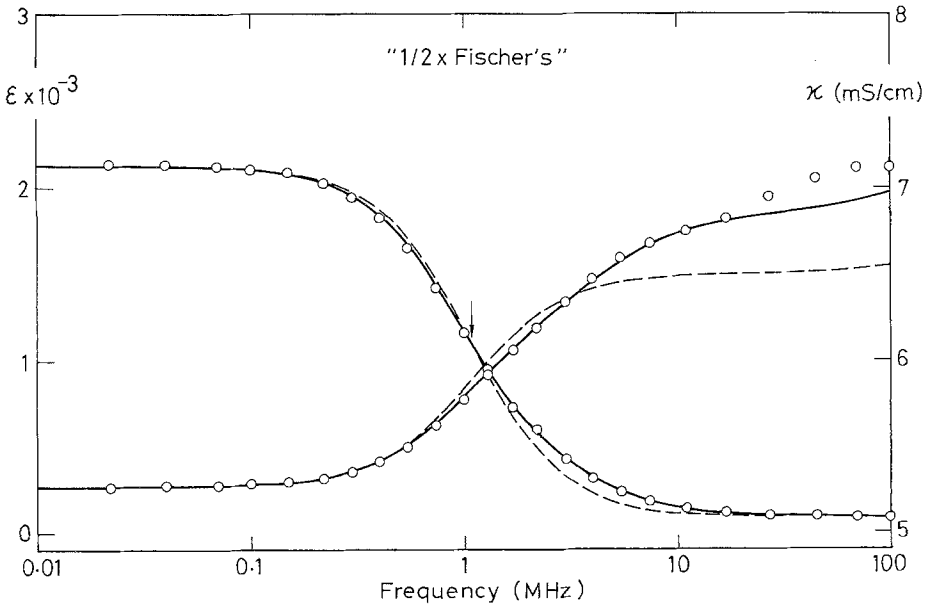

Fig. 7. Plots of dielectric constant (ε) and conductivity (κ), as functions of frequency, for a suspension of L 5178 Y cells in 1/2 × Fischer's medium (the case of $\kappa_a=6.60$ mS/cm in Table 2). Solid and dashed lines, as in Fig. 5

overall appearance of the dispersion curves resembles substantially that observed with the standard medium (Fig. 5) despite an approximately two-fold difference in the medium conductivity κ_a.

Unlike the above measurements, the one with $1/3 \times$ Fischer's was not free from time-dependent, significant increases in the suspension conductivity (especially at low frequencies) leading to poor reproducibility of the bridge measurements. This was probably caused by net ionic leakage out of cells exposed to such an extreme reduction in the ambient salt concentration as 1/3. For this reason it was impossible to get any reliable results in the case of $1/3 \times$ Fischer's.

Effect of Triton Treatment

In some experiments cells were suspended in a standard medium containing nonionic detergent, Triton X-100, as a membrane-lytic agent. Its critical lytic concentration varied between 0.01 and 0.05%, when the cells were incubated for 10 min at 25 °C, depending upon the volume concentration and condition of the cells examined. After treatment of the cells with a critical lytic concentration of the detergent, the so-far-established pattern of dielectric dispersion disappeared almost completely, although the definite nuclear structure still remained unaffected as checked by a high power phase microscopy.

Such a "dispersion-erasing" effect of Triton was observed also in its critical *sublytic* concentrations where no appreciable sign of lysis had yet been detectable in the outermost cytoplasmic membrane and much less in the nuclear membrane. These facts appear to indicate that it is very difficult, though not impossible, to carry out a precision measurement directly on bare nuclei isolated from living cells.

In light of these observations, we tried to estimate the electrical parameters of the cell interior by inspecting it from outside the limiting cell membrane with its physiological state maintained as intact as possible.

Results of Analysis

A) Simulation by the "Single-Shell" Model

An example of the $1 \times$ Fischer's case is depicted in Fig. 5. The dashed curves, the best fit in the sense of our criterion expressed previously [8], represent the ε- and κ-values that have been predicted through Eq. (1) by inserting the numerical parameters: $\varepsilon_s = 8.68$, $\varepsilon_i = 136$, $\kappa_i = 6.33$ mS/cm,

Table 2. Electrical parameters of L 5178 Y cells determined by using the "single-shell" model or th "double-shell" model

Suspend. medium	1 × Fischer's			1/2 × Fischer's			Mean ± SE
κ_a (mS/cm)	12.67	12.34	11.73	6.60	6.55	6.03	
Volume concn, Φ	0.155	0.176	0.150	0.144	0.138	0.162	
A) "Single-shell" model							
ε_s	8.68	8.80	9.60	9.01	8.25	8.60	8.82 ± 0.19
ε_i	136	158	137	135	137	131	139 ± 4
κ_i (mS/cm)	6.33	6.96	7.09	6.08	6.08	6.23	6.46 ± 0.18
B) "Double-shell" model							
ε_s	8.68	8.80	9.60	9.01	8.25	8.60	8.82 ± 0.19
κ_c (mS/cm)	10.7	11.6	11.7	10.5	10.4	10.9	11.0 ± 0.2
ε_n	16	15	20	22	18	25	19 ± 2
κ_n (mS/cm)	9×10^{-3}	12×10^{-3}	10×10^{-3}	6×10^{-3}	5×10^{-3}	1×10^{-3}	$7 \pm 2 \times 10$
ε_k	300	400	300	300	300	250	308 ± 20
κ_k (mS/cm)	7	7	9	7.5	8	9	8 ± 0.4
C_M (μF/cm²)	0.96	0.97	1.06	1.00	0.91	0.95	0.98 ± 0.02
C_N (μF/cm²)	0.35	0.33	0.44	0.49	0.40	0.55	0.43 ± 0.03
κ_c/κ_a	0.845	0.940	0.997	–	–	–	0.93 ± 0.04
κ_k/κ_c	0.65	0.60	0.77	0.71	0.77	0.83	0.72 ± 0.04

The parameters employed in the analysis are those of Table 1 and $\varepsilon_a = 77$ (observed) throughou The osmolarity of 1/2 × Fischer's medium was raised by addition of sucrose to make isosmotic with × Fischer's (310 ± 10 mOSM). Temperature, 25 ± 1 °C. Symbols defined as in Fig. 1.

etc. The systematic deviation of the predicted curves from the experimental points was not alleviated effectively even after due attention was paid to the possible contribution of heterogeneity in cell size (Appendix A). Another candidate mechanism capable of broadening the dispersion curves might be some distribution of electrical phase parameters, particularly that of κ_i (*cf.* Ref. 11); but we shall not refer to it without data in hand.

A similar trial was made on the 1/2 × Fischer's case, and the result is shown in Fig. 7 *(dashed curves)* and Table 2.

B) Simulation by the "Double-Shell" Model

When based on the "double-shell" model, the fitting improved appreciably as illustrated in Figs. 5 and 7 *(solid lines)*, covering almost all of the observed points except for those at frequencies in excess of 20 MHz. The reason for the remaining discrepancy of κ in the high frequency region is not known; it is highly probable, as already noted by Schwan, Takashima, Miyamoto and Stoeckenius [27], that poor performance of the RX-Meter at frequencies above several tens of MHz might have been responsible. In any case, if small residual deviations as seen in

Figs. 5 and 7 be permitted, we can successfully assign a plausible set of numerical parameters to the respective component phases of L5178Y cell. The results of such trials applied to three separate experiments for each medium condition are summarized in Table 2.

Of the eight parameters involved in the "double-shell" model, the outer shell conductivity κ_s and the cytoplasmic dielectric constant ε_c have been fixed at 8×10^{-7} mS/cm (corresponding to a membrane resistance of 1 kΩ cm^2) and 77 ($=\varepsilon_a$, the observed medium dielectric constant), respectively. As these values have not been actually determined but merely assumed for the purpose of calculation, the resulting estimates of the other phase parameters are inconclusive to that extent. Nevertheless, the choice of 1 kΩ cm^2 for membrane resistance appears not exceedingly out of proportion with the resistance values commonly encountered in cell membranes [3, 26]. Moreover, a choice of $\kappa_s=8\times10^{-6}$ mS/cm (corresponding to a membrane resistance of 100 Ω cm^2) did not fatally affect the assignment presented in Table 2. This statement is much more valid for $\kappa_s<8\times10^{-7}$ mS/cm (Paper *II*).

As will be discussed in Paper *II*, an actual determination of ε_k is related closely to that of ε_c, so that the estimate ($\varepsilon_k\simeq300$) would have been changed depending on a choice of ε_c substantially different from 77. However, we have chosen here a fixed value ($\varepsilon_c=77$) as a practical and reasonable assumption in that the resultant pattern of dispersion curves was virtually insensitive to changes in ε_c from 30 up to 200 (Paper *II*) and in that there has been no available evidence for ε_c to take a high value as much as several hundreds dielectric unit or more. Hence the whole body of the assignment given in Table 2 might be acceptable as being not too unrealistic.

Thus the following is concluded from the results in Table 2 (the "double-shell" model case): (i) the imposed, two-fold difference in the ambient salinity did not induce any systematic changes in the analyzed electrical parameters of the lymphoma cell, and (ii) each parameter averages $\varepsilon_s\simeq8.8$, $\varepsilon_n\simeq19$, $\varepsilon_k\simeq300$, $\kappa_c\simeq11$, $\kappa_n\simeq7\times10^{-3}$, and $\kappa_k\simeq8$ (κ's in mS/cm), with some derived data such as $C_M\simeq1.0$, $C_N\simeq0.4$ (both in μF/cm^2), $\kappa_c/\kappa_a\simeq0.9$ (with κ_a for 1 × Fischer's), and $\kappa_k/\kappa_c\simeq0.7$. Here, the specific capacities, C_M and C_N, referring respectively to the cellular and the nuclear membranes, have been calculated according to the equations:

$$C_M=\varepsilon_s\varepsilon_0/d \tag{5}$$

$$C_N=\varepsilon_n\varepsilon_0/d_n \tag{6}$$

where $\varepsilon_0=8.85\times10^{-8}$ μF/cm.

Discussion

Comparison of the "Single-Shell" and the "Double-Shell" Models

The results of our curve-fitting as shown in Figs. 5 and 7 clearly demonstrate that the "double-shell" model has an obvious advantage over the "single-shell" model in explaining the dielectric behavior shown by the cell population of lymphoid origin. The reason for such relative inadequacy of the "single-shell" model to the present case may be argued in the following way[3].

The Pauly-Schwan theory (Eq. (1)) for the "single-shell" model is written, in terms of two Debye-type expressions, as

$$\varepsilon = \frac{\Delta\varepsilon_P}{1+(\omega\tau_P)^2} + \frac{\Delta\varepsilon_Q}{1+(\omega\tau_Q)^2} + \varepsilon_h \tag{7}$$

where $\Delta\varepsilon_P$ and $\Delta\varepsilon_Q$ are the dielectric increments of P- and Q-dispersions [8], respectively, τ_P and τ_Q are their relaxation times, and ε_h is the limiting dielectric constant at high frequencies. Of the two quantities, $\Delta\varepsilon_P$ and $\Delta\varepsilon_Q$, the latter is assessed, as pointed out previously [8], to be negligible compared with the former when one considers the conditions that $d/D = 80\,\text{Å}/13\,\mu\text{m} \ll 1$ and $\kappa_s/\kappa_a = (8\times10^{-7}\,\text{mS/cm})/(\sim 10\,\text{mS/cm}) \ll 1$, in which all the numerical parameters pertain to the present cell system. Thus, under these conditions, Eq. (7) reduces to

$$\varepsilon = \frac{\Delta\varepsilon_P}{1+(\omega\tau_P)^2} + \varepsilon_h \tag{8}$$

suggesting that the major portion of the experimental points should conform to a curve characteristic of the simple Debye expression like Eq. (8) if the "single-shell" model were to be a good approximation.

Such a prediction was not realized, however, as illustrated in Figs. 5 and 7 *(dashed curves)*. Even if some distribution of relaxation times, say, that of a Cole-Cole type [4], is allowed to have taken place (as is suggested from Fig. 6), the "single-shell" model would not fully account for the observed dielectric dispersion curves, because if a Cole-Cole type distribution had been involved then the observed dielectric constants

3 Other lines of argument should include: (i) contributions of intracellular proteins and protein-bound water, and (ii) the possibility of frequency-dependent membrane parameters. However, we attempt here to focus upon the "shell models" which assume implicitly that all the parameters involved are independent of frequency and that interfacial polarization due to the layered structure is solely responsible for the observed dispersion characteristics.

should have traced a curve which is symmetric around the point of inflection (indicated by *arrow*) in the diagram of ε *vs.* log frequency (Figs. 5 and 7); this, however, was not the case either.

Taking into account the above together with the structural peculiarity of the cells examined, we adopted the "double-shell" model as a more favorable tool in analyzing the observed raw data of dielectric measurements.

Evaluation of the "Double-Shell" Model and Interpretation of the Analyzed Parameters

ε_s. The dielectric constant of the outermost phase ε_s is the only one parameter to which either model gave the same estimate with high precision. The membrane capacity C_M of 1 μF/cm^2, derived from ε_s, is in full accord with that of various cell membranes [3, 26].

κ_c. One of the most remarkable features of the "double-shell" model approach lies in its feasibility of discriminating κ_c from κ_n or κ_k. In fact, our new approach provided the assignment such as $\kappa_c = 11.0$, $\kappa_n = 7 \times 10^{-3}$ and $\kappa_k = 8$ (all in mS/cm), while the conventional "single-shell" approach could only provide a crude estimate of conductivity ($\kappa_i = 6.4$ mS/cm) for the cell interior as an apparently homogeneous phase.

The value of κ_c turned out very close to that of the physiological medium used (Table 2, κ_c/κ_a). This might be possibly related to the intracellular ion composition of L5178Y cells. Wotring Roti Roti and Rothstein [30] and Buckhold Shank and Smith [2] describe this cell line to contain 24–28 mM Na, 198–205 mM K, and 51 mM Cl as its major univalent ions. Although there is no direct evidence for these values to represent exclusively the cytoplasmic compartment since the analyses were made with the whole cell, one can still have a rough estimate for the concentration of osmotically active (free) ions in the cytoplasmic fluid of about 280 mM, which figure compares favorably with that of the standard medium (290 mM for 1 × Fischer's). Hence, subject to an allowance for the possibility that the cytoplasmic conductivity can be lower (because of relatively high viscosity and presumedly low ionic activity coefficient in protoplasm) than would be expected when the analytic concentration (280 mM) referred to a simple salt solution, our result ($\kappa_c/\kappa_a \simeq 0.9$) appears to fall within a quite reasonable range. In addition, it is inferred that a high degree of so-called "sequestration" of ions in the cytoplasmic compartment is unlikely if it were not for an uneven, cytoplasmic

accumulation of the intracellular ions. This point will be discussed in relation to an interpretation of the nucleus-related parameter κ_k.

ε_n and κ_n. Of particular interest is to compare the present results with those obtained by the microelectrode technique (for review, *see* Ref. 15). Loewenstein and Kanno [13, 14], studying the electrical properties of nuclei from several cell species, have reported that the specific resistances of nuclear envelope (R_N), with the exception of oocytes ($<0.001\,\Omega\,\mathrm{cm}^2$), center around $1\,\Omega\,\mathrm{cm}^2$ (salivary gland cells), which is considerably lower than those associated with the cell membrane. Our estimate of R_N for the lymphoid cell turned out to be $0.6\,\Omega\,\mathrm{cm}^2$, when calculated using $\kappa_n = 7 \times 10^{-3}\,\mathrm{mS/cm}$ and $d_n = 400\,\text{Å}$, in good agreement with the gland cell nuclei in the order of magnitude. Such a coincidence appears to support the general notion that $R_N \approx 1\,\Omega\,\mathrm{cm}^2$ in some somatic cells. As for the capacitive counterpart C_N, on the other hand, our method gave a value $\sim 0.4\,\mu\mathrm{F/cm}^2$ which is nearly one half of C_M, the cell membrane capacity. This is far smaller than the *apparent* capacitances calculated from time constants in gland cell nuclei [13] and rather resembles a figure ($\sim 0.5\,\mu\mathrm{F/cm}^2$) reported on mitochondrial limiting membranes [20]. Loewenstein and Kanno [13] advanced a possible explanation for the unusually large capacitance ($\sim 100\,\mu\mathrm{F/cm}^2$); they consider that the nuclear membrane may be extended by endoplasmic reticulum in the gland cell. On the other hand, there is a structural analogy between the nuclear and mitochondrial membranes in that the major portion of both systems consists of *double* membranes arranged in series, so that if each unit of the double membrane system has a capacitance of $\sim 1\,\mu\mathrm{F/cm}^2$ then the composite capacitance ought to be about $0.5\,\mu\mathrm{F/cm}^2$. An apparent discrepancy between our result and that of Loewenstein and Kanno [13] might be due to different techniques as well as different cell species employed.

In order to correlate ε_n and κ_n with the nuclear envelope structure, we attempted a calculation based on a model (Fig. 8) in which a "membrane-covered" portion is in parallel with lumped "pores" that occupy an areal fraction f over the entire nucleus surface. By using the notations defined in Fig. 8 and neglecting the possible interaction between neighboring pores [12], the complex dielectric constant of the overall envelope is expressed as

$$\varepsilon_n^* = f\varepsilon_{pore}^* + (1-f)\varepsilon_{m\text{-}c}^* \tag{9}$$

and

$$\frac{d_n}{\varepsilon_{m\text{-}c}^*} = \frac{2\delta_m}{\varepsilon_m^*} + \frac{\delta_{cist}}{\varepsilon_{cist}^*} \tag{10}$$

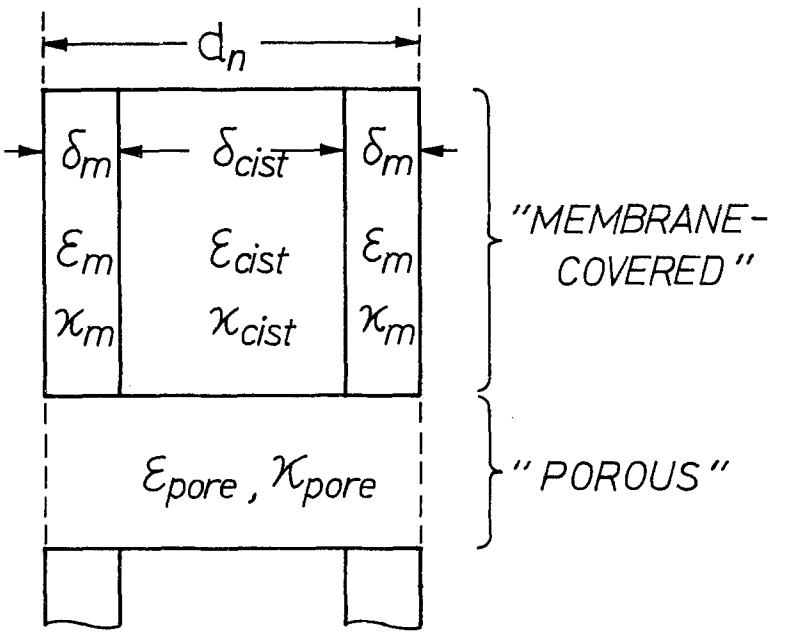

Fig. 8. Schematic profile of the nuclear envelope of L 5178 Y cells. The overall envelope is composed of two layers of unit membranes separated by "cisterna" and perforated by "pores"

where asterisks (*) denote the respective complex quantities defined, for example, $\varepsilon_n^* = \varepsilon_n + \kappa_n/j\omega\varepsilon_0$, and $\varepsilon_{m\text{-}c}$ stands for the composite dielectric constant of the "membrane-covered" area. The final expressions deduced from these relations on the reasonable assumption that $\varepsilon_m = \varepsilon_s$, $\kappa_m = \kappa_s \ll \kappa_{cist}$, and $\delta_m = d$, together with the numerical results for ε_n and κ_n (Table 2), are written (for derivation, *see* Appendix B) as

$$\varepsilon_{pore} = 22 - 2.8/f \tag{11}$$

$$\kappa_{pore}(\text{in mS/cm}) = (7.2 \times 10^{-3})/f. \tag{12}$$

Recalling the constraints that $\varepsilon_{pore} > 1$ and $0 < f < 0.60$ ($f = 0.60$ means the closest packing), one obtains, as a requirement from Eqs. (11) and (12),

$$1 < \varepsilon_{pore} < 17 \tag{13}$$

$$0.012 < \kappa_{pore} < 0.055 \quad (\text{in mS/cm}) \tag{14}$$

$$0.13 < f < 0.60. \tag{15}$$

Now, with the aid of electron micrographs (Fig. 4), another estimate of f, the pore fraction, is made as follows. Fig. 4 shows that the pore diameter averages 1000 Å with a minimum center-to-center distance of 1500 Å. If we assume a hexagonal distribution [29] for the pores in

question, these values give rise to an f-value of 0.27, a result completely satisfying relation (15). Next, insertion of $f=0.27$ into Eqs. (11) and (12) gives an electrical correlate of the "nuclear pores" such as $\varepsilon_{pore} \simeq 12$ and $\kappa_{pore} \simeq 0.03$ mS/cm, the latter being two to three orders of magnitude smaller than κ_c or κ_k. Such a result appears to confirm, at least qualitatively, the finding of Loewenstein and Kanno [13] who for the first time pointed out the essential role played by the "pore material" in rendering a diffusion barrier nature to the nuclear envelope.

The interpretation of $\varepsilon_{pore} \simeq 12$ remains an open question; at best, it is conjectured that the nuclear pores might be abundantly filled up with a certain kind of polymer substance like protein or polysaccharide, or a combination thereof, either of which has a relatively low dielectric constant compared with that of water ($\varepsilon \simeq 80$).

ε_k and κ_k. On account of very leaky and fragile nature inherent in the nucleus envelope [7] any *in situ* information of the state of nuclear ions, especially that of small ions such as Na^+ and K^+, has been considered almost inaccessible by the conventional chemical-analytical or micropuncture techniques as applied to the nuclei isolated (or semi-isolated) under an artificial condition. One of the objectives of the present study was to challenge these difficulties. Indeed, the approach presented above, albeit immature at present, did disclose some knowledge of the nucleus interior, that is, $\varepsilon_k \simeq 300$ and $\kappa_k \simeq 8$ mS/cm.

The determination of ε_k might have been spurious because of its strong dependence upon the assumed value for ε_c, the cytoplasmic dielectric constant, as stated in Paper *II*. Moreover, the relative insensitivity of the dispersion curves to changes in ε_k (Paper *II*) makes the determination even less convincing. For all these, however, if such an ε_k should be any indication of karyoplasmic dielectric properties, it is tempting to correlate the ε_k with the nuclear content of DNA which is known to have a large dipole moment of 10^4–10^6 Debye [9, 23, 28]. By using an analytical value for the L5178Y cells (7 pg DNA/nucleus) reported by Defendi and Manson [5] in conjunction with our nuclear volume data (0.37 pl/nucleus), the order of the DNA concentration in question is calculated to be 20 g/liter. This figure favors, qualitatively at least and in case the nuclear DNA plays a role in building up ε_k, the above estimate of ε_k which is apparently higher than that of water[4].

4 A recent experiment [23] shows: (i) ε of aqueous DNA solutions (concn, 0.1–0.5 g/liter) amounts to an order of 10^3–10^4 in an ambient univalent salt of millimolar concentrations, (ii) ε increases with increasing concentration of DNA, and (iii) elevated concentration of added salt decreases ε and increases characteristic frequency.

Last but not of least importance is a brief remark on κ_k. As seen in Table 2, our analysis gave a ratio $\kappa_k/\kappa_c \simeq 0.7$. The most straightforward interpretation of this value would be such that the total ion activity in the nucleoplasm is lower by approx. 30% than in the cytoplasm if the conductivity can be a faithful measure of total ion activity as in an ideal ionic solution. It should be noted, however, this interpretation does not necessarily mean that the nuclear compartment contained less ions than the cytoplasm. Conversely, more excess ions could have been distributed in nucleus than in cytoplasm just as is the case with many other cell species (for references, *see*, e.g., [18]). If so, then the nuclear ions conceivably underwent a higher degree of "sequestration" than the cytoplasmic ones[5]. Such a situation could have occurred as a result of, say, preferential binding of nuclear cations such as Na^+ and K^+ to anionic sites of nuclear macromolecules.

Concluding Remarks

As described above, the assignment as a whole appears fairly reasonable and realistic. This in turn favors the use of the "double-shell" model rather than the "single-shell" model as far as the present lymphoid cells are concerned. It is also indicated that a further refinement of the dielectric dispersion method would reveal more information about the cell interior including various membranous structures, the access to which has been highly limited to date.

We wish to thank Dr. N. Koizumi for valuable suggestions on the bridge measurements and Dr. G. Roy for critical reading of the manuscript. Dr. H. Ozaki's collaboration in electron microscopy is gratefully acknowledged.

Appendix A

On assuming that the superposition principle applies to a relationship between ε^* and differential volume fraction Φ_j (where $\Sigma\Phi_j = \Phi$), Eq. (1) can be extended to include a distribution of size parameter R_j's (R_j = inner radius of particles of class j) as

$$\frac{\varepsilon_a^* - \varepsilon^*}{2\varepsilon_a^* + \varepsilon^*} = \sum_j \frac{(\varepsilon_a^* - \varepsilon_s^*)(2\varepsilon_s^* + \varepsilon_i^*) + (\varepsilon_a^* + 2\varepsilon_s^*)(\varepsilon_s^* - \varepsilon_i^*)(1 + 2d/R_j)^{-3}}{(2\varepsilon_a^* + \varepsilon_s^*)(2\varepsilon_s^* + \varepsilon_i^*) + 2(\varepsilon_a^* - \varepsilon_s^*)(\varepsilon_s^* - \varepsilon_i^*)(1 + 2d/R_j)^{-3}} \Phi_j .$$

5 As discussed in detail by Pauly and Schwan [22], another factor to retard karyoplasmic ion mobility, and hence the conductivity κ_k, is supposedly a high viscosity of nucleus interior that contains such a high concentration of nuclear macromolecules.

Then one may compute ε and κ for any polydisperse system by using its size histogram such as shown in Fig. 3*b*. A similar attempt has been made in our previous paper on synaptosomes [11].

Appendix B

Derivation of Eqs. (11) *and* (12)

By definition, Eq. (9) is rewritten as

$$\varepsilon_n+\frac{\kappa_n}{j\omega\varepsilon_0}=f\varepsilon_{pore}+\frac{f\kappa_{pore}}{j\omega\varepsilon_0}+(1-f)\,\varepsilon_{m\text{-}c}+\frac{(1-f)\kappa_{m\text{-}c}}{j\omega\varepsilon_0}. \tag{B 1}$$

Comparison with respect to the real and the imaginary parts of Eq. (B 1) gives:

$$\varepsilon_n=f\varepsilon_{pore}+(1-f)\varepsilon_{m\text{-}c}, \tag{B 2}$$

$$\kappa_n=f\kappa_{pore}+(1-f)\kappa_{m\text{-}c}. \tag{B 3}$$

Similarly, from Eq. (10), we have

$$\frac{\varepsilon_{m\text{-}c}d_n}{\varepsilon_{m\text{-}c}^2+(\kappa_{m\text{-}c}/\omega\varepsilon_0)}=\frac{2\varepsilon_m\delta_m}{\varepsilon_m^2+(\kappa_m/\omega\varepsilon_0)^2}+\frac{\varepsilon_{cist}\delta_{cist}}{\varepsilon_{cist}^2+(\kappa_{cist}/\omega\varepsilon_0)^2}, \tag{B 4}$$

$$\frac{\kappa_{m\text{-}c}d_n}{\varepsilon_{m\text{-}c}^2+(\kappa_{m\text{-}c}/\omega\varepsilon_0)^2}=\frac{2\kappa_m\delta_m}{\varepsilon_m^2+(\kappa_m/\omega\varepsilon_0)^2}+\frac{\kappa_{cist}\delta_{cist}}{\varepsilon_{cist}^2+(\kappa_{cist}/\omega\varepsilon_0)^2}. \tag{B 5}$$

Our concern here is to obtain the relations at static field since the parameters are defined as such, so that at $\omega\to 0$ Eqs. (B 4) and (B 5) reduce respectively to

$$\frac{\varepsilon_{m\text{-}c}d_n}{\kappa_{m\text{-}c}^2}=\frac{2\varepsilon_m\delta_m}{\kappa_m^2}+\frac{\varepsilon_{cist}\delta_{cist}}{\kappa_{cist}^2} \tag{B 6}$$

and

$$\frac{d_n}{\kappa_{m\text{-}c}}=\frac{2\delta_m}{\kappa_m}+\frac{\delta_{cist}}{\kappa_{cist}}. \tag{B 7}$$

On assuming here that $\kappa_m\ll\kappa_{cist}$, as stated in the text, the above two relations can be approximated by

$$\varepsilon_{m\text{-}c}=\varepsilon_m\left(\frac{2\delta_m}{d_n}\right)\left(\frac{\kappa_{m\text{-}c}}{\kappa_m}\right)^2 \tag{B 8}$$

and

$$\frac{\kappa_{m\text{-}c}}{\kappa_m}=\frac{d_n}{2\delta_m}. \tag{B 9}$$

Combination of Eqs. (B 8) and (B 9) gives

$$\varepsilon_{m\text{-}c}=\varepsilon_m d_n/2\delta_m. \tag{B 10}$$

By substituting Eqs. (B 10) and (B 9), respectively, into Eqs. (B 2) and (B 3), as well as recalling the assumptions that $\varepsilon_m=\varepsilon_s$, $\kappa_m=\kappa_s$ and $\delta_m=d$ together with their numerical values listed in Tables 1 and 2, we can finally derive text Eqs. (11) and (12).

Appendix C

Assessment of Dispersion Magnitude for ε_n and κ_n

Our standpoint throughout this article is such that all the phase parameters included in the "shell models" (Fig. 1) should be independent of the applied frequency. It is necessary therefore to assess the magnitude of variation of ε_n (and of κ_n), if any, as a function of frequency, in case the nuclear envelope phase (for which ε_n and κ_n stand) is no longer approximated by a single, homogeneous entity but by a combination of its substructures such as depicted in Fig. 8. In other words, we cannot go into any details beyond the gross knowledge of $\varepsilon_n^*(\equiv\varepsilon_n+\kappa_n/j\omega\varepsilon_0)$ if either or both of these nuclear envelope parameters should show a strong frequency dependence as a result of subdividing ε_n^* into ε_{pore}^*, ε_{cist}^*, and ε_m^* (*see* Fig. 8).

For the purpose of numerical assessment it is advantageous to rewrite text Eq. (10) as

$$\varepsilon_{m\text{-}c}^*=\varepsilon_h+\frac{\varepsilon_l-\varepsilon_h}{1+j\omega\tau}+\frac{\kappa_l}{j\omega\varepsilon_0}, \tag{C 1}$$

where

$$\varepsilon_h=\frac{\varepsilon_m\varepsilon_{cist}}{\varepsilon_{cist}+\phi(\varepsilon_m-\varepsilon_{cist})}, \tag{C 2}$$

$$\varepsilon_l-\varepsilon_h=\frac{\phi(1-\phi)(\varepsilon_m\kappa_{cist}-\varepsilon_{cist}\kappa_m)^2}{[\varepsilon_{cist}+\phi(\varepsilon_m-\varepsilon_{cist})][\kappa_{cist}+\phi(\kappa_m-\kappa_{cist})]^2}, \tag{C 3}$$

$$\kappa_l=\frac{\kappa_m\kappa_{cist}}{\kappa_{cist}+\phi(\kappa_m-\kappa_{cist})}, \tag{C 4}$$

$$\tau \equiv \frac{1}{2\pi f_0} = \frac{\varepsilon_{cist} + \phi(\varepsilon_m - \varepsilon_{cist})}{\kappa_{cist} + \phi(\kappa_m - \kappa_{cist})} \cdot \varepsilon_0, \tag{C 5}$$

and

$$\phi = \delta_{cist}/d_n. \tag{C 6}$$

Here, the subscripts, l and h, refer respectively to the low- and high-frequency limiting values to be attained by that particular portion ("m-c"); τ is relaxation time; and f_0 is critical frequency.

Separating the real and imaginary parts of Eq. (C 1),

$$\varepsilon^*_{m\text{-}c} = \varepsilon_h + \frac{\varepsilon_l - \varepsilon_h}{1+(\omega\tau)^2} + \frac{1}{j\omega\varepsilon_0} \cdot \left(\frac{\omega^2 \tau \varepsilon_0 (\varepsilon_l - \varepsilon_h)}{1+(\omega\tau)^2} + \kappa_l \right). \tag{C 7}$$

On the other hand, ε^*_n is expressed as

$$\varepsilon^*_n = \varepsilon_n(\omega) + \kappa_n(\omega)/j\omega\varepsilon_0. \tag{C 8}$$

Substituting Eq. (C 7) into text Eq. (9) and comparing Eq. (C 8) with text Eq. (9), we finally get the expressions:

$$\varepsilon_n(\omega) = f\varepsilon_{pore} + (1-f)\varepsilon_h + (1-f) \cdot \frac{\varepsilon_l - \varepsilon_h}{1+(\omega\tau)^2}, \tag{C 9}$$

$$\kappa_n(\omega) = f\kappa_{pore} + (1-f)\,\kappa_l + (1-f) \cdot \frac{\omega^2 \tau \varepsilon_0 (\varepsilon_l - \varepsilon_h)}{1+(\omega\tau)^2}. \tag{C 10}$$

Table 3. Frequency-dependent variation of ε_n and κ_n

κ_{cist} (mS/cm)	Frequency (MHz)				Critical frequency f_0 (MHz)
	0.1	1	10	100	
	$\varepsilon_n(\omega)$				
10	19.3	19.3	19.3	18.8	199
1	19.3	19.3	18.8	17.0	19.9
0.1	19.3	18.8	17.0	16.9	1.99
0.01	18.8	17.0	16.9	16.9	0.199
	$\kappa_n(\omega)$ in μS/cm				
10	7.20	7.21	7.86	59.9	
1	7.20	7.27	12.4	29.4	
0.1	7.21	7.73	9.72	9.82	
0.01	7.25	7.45	7.46	7.46	

$\varepsilon_n(\omega)$, $\kappa_n(\omega)$, and f_0 were calculated from Eqs. (C 9), (C 10), and (C 5) by using: $\varepsilon_{pore} = 11.8$; $\kappa_{pore} = 0.0268$ mS/cm; $\varepsilon_{cist} = 77$; $\kappa_{cist} = 10$, 1, 0.1, or 0.01 mS/cm; $f = 0.269$; and $\psi = 0.6$.

Now we can calculate the values of ε_n and κ_n on the basis of the model shown in Fig. 8. The result is given in Table 3. Note that the κ_{cist}-values were chosen for probing purpose.

Now it is apparent that subdivision of the nuclear envelope phase gives rise to slight, but definite, frequency-dependent variation in the resultant values of ε_n and κ_n. However, as far as the present frequency range (0.1–100 MHz) is concerned, the magnitude of variation is not so great as to seriously affect our rather qualitative estimates of ε_{pore} and κ_{pore}.

References

1. Asami, K., Hanai, T., Koizumi, N. 1976. Dielectric properties of yeast cells. *J. Membrane Biol.* **28**:169
2. Buckhold Shank, B., Smith, N.E. 1974. Characterization of the steady state in mouse lymphoblasts cultured in hypotonic medium. *Biochim. Biophys. Acta* **367**:59
3. Cole, K.S. 1968. Membranes, Ions and Impulses. University of California Press, Berkeley
4. Cole, K.S., Cole, R.H. 1941. Dispersion and absorption in dielectrics. I. Alternating current characteristics. *J. Chem. Phys.* **9**:341
5. Defendi, V., Manson, L.A. 1963. Analysis of the life-cycle in mammalian cells. *Nature (London)* **198**:359
6. Eaton, M.S., Scala, A.R., Jewell, M. 1959. Methods for measuring viability of ascites cells. Dye exclusion and respiration as affected by depletion, poisons and viruses. *Cancer Res.* **19**:945
7. Franke, W.W., Scheer, U. 1974. Structures and functions of the nuclear envelope. *In:* The Cell Nucleus, H. Busch, editor. Vol. 1, p. 219. Academic Press, New York
8. Hanai, T., Koizumi, N., Irimajiri, A. 1975. A method for determining the dielectric constant and conductivity of membrane-bounded particles. *Biophys. Struct. Mechan.* **1**:285
9. Hanss, M., Bernengo, J.C. 1973. Dielectric relaxation and orientation of DNA molecules. *Biopolymers* **12**:2151
10. Irimajiri, A., Hanai, T., Inouye, A. 1975. Evaluation of a conductometric method to determine the volume fraction of the suspensions of biomembrane-bounded particles. *Experientia* **31**:1373
11. Irimajiri, A., Hanai, T., Inouye, A. 1975. Dielectric properties of synaptosomes isolated from rat brain cortex. *Biophys. Struct. Mechan.* **1**:273
12. Kanno, Y., Loewenstein, W.R. 1963. A study of the nucleus and cell membranes of oocytes with an intracellular electrode. *Exp. Cell Res.* **31**:149
13. Loewenstein, W.R., Kanno, Y. 1963. Some electrical properties of a nuclear membrane examined with a microelectrode. *J. Gen. Physiol.* **46**:1123
14. Loewenstein, W.R., Kanno, Y. 1963. The electrical conductance and potential across the membrane of some nuclei. *J. Cell Biol.* **16**:421
15. Loewenstein, W.R., Kanno, Y., Ito, S. 1966. Permeability of nuclear membranes. *Ann. N.Y. Acad. Sci.* **137**:708
16. Luft, J.H. 1961. Improvements in epoxy resin embedding method. *J. Biophys. Biochem. Cytol.* **9**:409
17. Malenkov, A.G., Voeikov, V.L., Ovchinikov, Yu.A. 1972. Electroconductivity changes during the mitotic cycle in Ehrlich ascites tumor cells. *Biochim. Biophys. Acta* **255**:304

18. Moore, R.D., Morrill, G.A. 1976. A possible mechanism for concentrating sodium and potassium in the cell nucleus. *Biophys. J.* **16**:527
19. Pauly, H. 1963. Über die elektrische Kapazität der Zellmembran und die Leitfähigkeit des Zytoplasmas von Ehrlich-Aszitestumorzellen. *Biophysik* **1**:143
20. Pauly, H., Packer, L., Schwan, H.P. 1960. Electrical properties of mitochondrial membranes. *J. Biophys. Biochem. Cytol.* **7**:589
21. Pauly, H., Schwan, H.P. 1959. Über die Impedanz einer Suspension von kugelförmigen Teilchen mit einer Schale. *Z. Naturforsch.* **14b**:125
22. Pauly, H., Schwan, H.P. 1966. Dielectric properties and ion mobility in erythrocytes. *Biophys. J.* **6**:621
23. Sakamoto, M., Kanda, H., Hayakawa, R., Wada, Y. 1976. Dielectric relaxation of DNA in aqueous solutions. *Biopolymers* **15**:879
24. Schwan, H.P. 1957. Electrical properties of tissue and cell suspensions. *In:* Advances in Biological and Medical physics. J.H. Lawrence and C.A. Tobias, editors. Vol. 5, p. 147. Academic Press, New York
25. Schwan, H.P. 1963. Determination of biological impedances. *In:* Physical Techniques in Biological Research. W.L. Nastuk, editor. Vol. 6, Part B, p. 323. Academic Press, New York
26. Schwan, H.P., Cole, K.S. 1960. Bioelectricity: Alternating current admittance of cells and tissues. *In:* Medical Physics. O. Glasser, editor. Vol. 3, p. 52. Yearbook Publishers, Chicago
27. Schwan, H.P., Takashima, S., Miyamoto, V.K., Stoeckenius, W. 1970. Electrical properties of phospholipid vesicles. *Biophys. J.* **10**:1102
28. Takashima, S. 1966. Dielectric dispersion of deoxyribonucleic acid. II. *J. Phys. Chem.* **70**:1372
29. Wiener, J., Spiro, D., Loewenstein, W.R. 1965. Ultrastructure and permeability of nuclear membranes. *J. Cell Biol.* **27**:107
30. Wotring Roti Roti, L., Rothstein, A. 1973. Adaptation of mouse leukemic cells (L 5178 Y) to anisotonic media. I. Cell volume regulation. *Exp. Cell Res.* **79**:295